ЖУРНАЛ ФІЗИЧНИХ ДОСЛІДЖЕНЬ
Т. 13, № 4 (2009) 4703(8 с.)

JOURNAL OF PHYSICAL STUDIES
v. 13, No. 4 (2009) 4703(8 p.)

TOTAL ELECTRONIC RAMAN SCATTERING IN THE CHARGE-DENSITY-WAVE PHASE OF THE SPINLESS FALICOV–KIMBALL MODEL

O. P. Matveev[1], A. M. Shvaika[1], J. K. Freericks[2]
[1] *Institute for Condensed Matter Physics of the National Academy of Sciences of Ukraine, 1, Svientsitskii St., 79011 Lviv, Ukraine*
[2] *Department of Physics, Georgetown University, Washington, DC 20057, USA*
(Received October 16, 2009)

The total electronic Raman scattering spectrum, including the nonresonant, mixed and resonant components, is determined for the charge–density–wave (CDW) phase of the spinless Falicov–Kimball model at half filling within dynamical mean-field theory. Its frequency dependence is investigated for different values of the energy of the incident photons. The spectra reflect different structures in the density of states and how they are modified by screening and resonance effects. The calculations are performed for the B_{1g}, B_{2g} and A_{1g} symmetries (which are typically examined in the experiment). Our results for the resonance effects of the Raman spectra, found by tuning the energy of the incident photons, give some information about the many-body charge dynamics of the CDW-ordered phase.

Key words: Dynamical mean-field theory, electronic Raman scattering, charge-density-wave phase.

PACS number(s): 71.10.Fd, 71.45.Lr, 78.30.−j

I. INTRODUCTION

Experiments on inelastic light scattering are employed to learn about the complicated charge dynamics of a wide class of strongly correlated electronic materials. The photon couples to the charge excitations during the inelastic scattering process and directly probes the charge excitations of different symmetries. In this work, we study the strongly correlated electron systems with charge-density-wave (CDW) ordering. CDW systems possess a static spatial modulation of the electronic charge with some spatial ordering wavevector. Since the underlying ionic cores are charged, they also respond to this charge modulation of the electron density and often create a distorted lattice structure that follows the modulated charge order of the electrons. A direct measurement of the lattice distortion due to the ionic displacement is often the best way to measure the presence of CDW order; it is more difficult to directly measure the electronic charge modulation in the material.

In the present work, we investigate how CDW order affects inelastic light scattering experiments by utilizing dynamical mean-field theory (DMFT) to exactly solve the total electronic Raman spectra. Since inelastic Raman scattering is sensitive to different symmetry charge modulations (when polarizers are used on the incident and scattered light) it can provide information about the symmetry of the CDW state and of the many-body charge excitations. We expect our results should be relevant to different experimental systems that display charge-density-wave order via nesting on a bipartite lattice at half filling, especially in compounds which are three-dimensional like $BaBiO_3$ and $Ba_{1-x}K_xBiO_3$ [1–3] because DMFT is most accurate in higher spatial dimensions; it may also be relevant to some layered two-dimensional systems, at least in a semi-quantitative fashion. Our work is the next step in recent results on transport, optical conductivity, and nonresonant inelastic X-ray scattering in CDW systems [4–6] to the realm of resonant inelastic light scattering. Since experimental inelastic light scattering work on CDW systems was focused on the Raman scattering of the soft phonon modes, future experimental work should examine the electronic scattering directly. Hence this work has the potential to be directly relevant to the next generation of Raman experiments on strongly correlated CDW materials.

One of the simplest models which posseses static CDW ordering at low temperature is the Falicov–Kimball model [7]. Historically, this model was introduced in 1969 to describe metal-insulator transitions in rare-earth compounds and transition-metal oxides. Later, it was found that it has an exact solution within DMFT [8] (for a review see Ref. [9]). The Falicov–Kimball model has two kinds of particles: itinerant electrons and localized electrons. Mobile electrons hop from site to site with a hopping integral between nearest neighbors and they interact with the localized electrons when both sit on the same site (the interaction energy is U); we denote the itinerant electron creation (annihilation) operator at site i by $\hat{d}_i^\dagger$ ($\hat{d}_i$) and the local electron creation (annihilation) operator at site i by $\hat{f}_i^\dagger$ ($\hat{f}_i$). The model has commensurate (chessboard) CDW order at half filling and this is the main property we exploit here. Brandt and Mielsch determined the formalism for calculating the ordered-phase Green's functions [10] shortly after Metzner and Vollhardt introduced the idea of the many-body problem simplifying in large dimensions [11]. The CDW order parameter is known to display anomalous behavior at weak coupling [12, 13], and higher-period ordered phases exist on the Bethe lattice [14].

II. DMFT FOR THE CDW PHASE OF THE FALICOV–KIMBALL MODEL

As mentioned above, the Falicov–Kimball model possesses the possibility for a transition into a commensurate CDW phase with doubly modulated (chessboard-like) density of charge, when both the itinerant and localized particles are half-filled. Since the hypercubic lattice is a bipartite lattice, implying that it is separated into two sublattices (called A and B) with the nearest-neighbor hopping being nonzero only between the different sublattices, the CDW order corresponds to the case where the average filling of the electrons remains uniform on each sublattice, but changes from one sublattice to another. We start by writing the Falicov–Kimball model Hamiltonian as the sum of its local and nonlocal parts

$$\hat{H} = \sum_{ia} \hat{H}_i^a - \sum_{ijab} t_{ij}^{ab} \hat{d}_{ia}^\dagger \hat{d}_{jb}, \tag{1}$$

where i and $a = A$ or B are the site and sublattice indices, respectively, and t_{ij}^{ab} is the hopping matrix, which is nonzero only between different sublattices ($t_{ij}^{AA} = t_{ij}^{BB} = 0$). The local Hamiltonian is equal to

$$\hat{H}_i^a = U \hat{n}_{id}^a \hat{n}_{if}^a - \mu_d^a \hat{n}_{id}^a - \mu_f^a \hat{n}_{if}^a; \tag{2}$$

with the number operators of the itinerant and localized electrons given by $\hat{n}_{id} = \hat{d}_i^\dagger \hat{d}_i$ and $\hat{n}_{if} = \hat{f}_i^\dagger \hat{f}_i$, respectively. Note that we have introduced different chemical potentials for the different sublattices. This is convenient for computations, because it allows us to work with a fixed order parameter, rather than iterating the DMFT equations to determine the order parameter. That method of iterative solution is subject to critical slowing down near T_c, while working with a fixed order parameter is not. The equilibrium solution occurs when the chemical potential is uniform throughout the system ($\mu_d^A = \mu_d^B$ and $\mu_f^A = \mu_f^B$), which is the unique condition used to find the order parameter at a given temperature.

We apply the DMFT, which provides an exact solution for the Falicov–Kimball model in the limit of infinite spatial dimensions. In contrast to the uniform case [15, 16], in the CDW phase, the DMFT equations become matrix equations. Since the DMFT solutions for the chessboard phase are described in detail in previous work [5, 6], we concentrate only on a few basic points as a summary and to establish our notation. The first step of DMFT is to scale the hopping matrix element as $t = t^*/2\sqrt{D}$ [11] (we use $t^* = 1$ as the unit of energy) and then take the limit of infinite dimensions $D \to \infty$. The self-energy is then local:

$$\Sigma_{ij}^{ab}(\omega) = \Sigma^a(\omega) \delta_{ij} \delta_{ab}, \tag{3}$$

and in the case of two sublattices has two values $\Sigma^A(\omega)$ and $\Sigma^B(\omega)$. Now, we can write the solution of the Dyson equation (in momentum space) in a matrix form

$$\mathbf{G}_{\boldsymbol{k}}(\omega) = \left[\mathbf{z}(\omega) - \mathbf{t}_{\boldsymbol{k}}\right]^{-1}, \tag{4}$$

where the irreducible part $\mathbf{z}(\omega)$ and hopping term $\mathbf{t}_{\boldsymbol{k}}$ are represented by the following 2×2 matrices:

$$\mathbf{z}(\omega) = \begin{pmatrix} \omega + \mu_d^A - \Sigma^A(\omega) & 0 \\ 0 & \omega + \mu_d^B - \Sigma^B(\omega) \end{pmatrix}, \tag{5}$$

$$\mathbf{t}_{\boldsymbol{k}} = \begin{pmatrix} 0 & \epsilon_{\boldsymbol{k}} \\ \epsilon_{\boldsymbol{k}} & 0 \end{pmatrix},$$

with $\epsilon_{\boldsymbol{k}} = -t^* \lim_{D\to\infty} \sum_{i=1}^D \cos(k_i)/\sqrt{D}$.

The second step of DMFT is to map the lattice Green's function onto a local problem by means of the dynamical mean field. Since there are two sublattices, a dynamical mean field $\lambda^a(\omega)$ is introduced on each of them. As a result, the local lattice Green's function on each sublattice becomes:

$$G^{aa}(\omega) = \frac{1}{\omega + \mu_d^a - \Sigma^a(\omega) - \lambda^a(\omega)}. \tag{6}$$

The third equation that closes the system of equations for $G^{aa}(\omega)$, $\Sigma^a(\omega)$ and $\lambda^a(\omega)$ is obtained from the condition that the local Green's function is defined as the Green's function of an impurity problem with the same dynamical mean field $\lambda^a(\omega)$. Such a problem can be exactly solved for the Falicov–Kimball model and the result is equal to

$$G^{aa}(\omega) = \frac{1 - n_f^a}{\omega + \mu_d^a - \lambda^a(\omega)} + \frac{n_f^a}{\omega + \mu_d^a - U - \lambda^a(\omega)}, \tag{7}$$

where n_f^a is an average concentration of the localized electrons on sublattice a which is found from the equilibrium condition of a uniform chemical potential ($\mu_f^A - \mu_f^B = 0$).

These equations are self-consistently solved numerically. In Ref. [5], we analyzed the evolution of the DOS in the CDW-ordered phase. We summarize the main points which are needed here. At $T = 0$, a real gap develops of magnitude U with square root singularities at the band edges. As the temperature increases, the system develops substantial subgap DOS which are thermally activated within the ordered phase until T is raised high enough that the system enters the normal phase. Plots of the DOS can be found in Ref. [5]. Note that the singular behavior occurs for one of the "inner" band edges on each sublattice, and that the subgap states develop very rapidly as the temperature rises. Furthermore, at half filling the DOS on each sublattice is related to the DOS on the other sublattice by a reflection about $\omega = 0$.

III. INELASTIC LIGHT SCATTERING

For an electronic system with nearest-neighbor hopping, the interaction with a weak external transverse electromagnetic field determined by the vector potential $\boldsymbol{A}$ is described by the Hamiltonian [17, 18]:

$$H_{\text{int}} = -\frac{e}{\hbar c} \sum_{\boldsymbol{k}} \boldsymbol{j}(\boldsymbol{k}) \cdot \boldsymbol{A}(-\boldsymbol{k}) + \frac{e^2}{2\hbar^2 c^2} \sum_{\boldsymbol{k}\boldsymbol{k}'} A_\alpha(-\boldsymbol{k}) \gamma_{\alpha,\beta}(\boldsymbol{k} + \boldsymbol{k}') A_\beta(-\boldsymbol{k}'), \tag{8}$$

where the number current operator and stress tensor for itinerant electrons are equal to

$$j_\alpha(\boldsymbol{q}) = \sum_{ab\boldsymbol{k}} \frac{\partial t_{ab}(\boldsymbol{k})}{\partial k_\alpha} \hat{d}_a^\dagger(\boldsymbol{k}+\boldsymbol{q}/2)\hat{d}_b(\boldsymbol{k}-\boldsymbol{q}/2) \quad \text{and} \quad \gamma_{\alpha,\beta}(\boldsymbol{q}) = \sum_{ab\boldsymbol{k}} \frac{\partial^2 t_{ab}(\boldsymbol{k})}{\partial k_\alpha \partial k_\beta} \hat{d}_a^\dagger(\boldsymbol{k}+\boldsymbol{q}/2)\hat{d}_b(\boldsymbol{k}-\boldsymbol{q}/2), \tag{9}$$

respectively. Here $t_{ab}(\boldsymbol{k})$ are the components of the 2×2 hopping matrix in Eq. (5). The formula for the inelastic light scattering cross-section derived by Shastry and Shraiman is equal to [17, 18]

$$R(\boldsymbol{q},\Omega) = 2\pi \sum_{i,f} \frac{e^{-\beta\varepsilon_i}}{Z} \delta(\varepsilon_f - \varepsilon_i - \Omega) \left| g(\boldsymbol{k}_i) g(\boldsymbol{k}_f) e_\alpha^i e_\beta^f \left\langle f \left| \hat{M}^{\alpha\beta}(\boldsymbol{q}) \right| i \right\rangle \right|^2 . \tag{10}$$

It describes the scattering of band electrons by photons with $\Omega = \omega_i - \omega_f$ and $\boldsymbol{q} = \boldsymbol{k}_i - \boldsymbol{k}_f$ being the transferred energy and momentum, respectively, $\boldsymbol{e}^{i(f)}$ is the polarization of the initial (final) states of the photons and $\varepsilon_{i(f)}$ denotes the electronic eigenstates. The quantity $g(\boldsymbol{q}) = (hc^2/V\omega_{\boldsymbol{q}})^{1/2}$ is called the "scattering strength" with $\omega_{\boldsymbol{q}} = c|\boldsymbol{q}|$, and $Z = \mathrm{Tr}\, \exp(-\beta\hat{H})$ the partition function. The scattering operator $\hat{M}(\boldsymbol{q})$ is constructed from both the number current operator and the stress tensor; it has both nonresonant and resonant contributions

$$\left\langle f \left| \hat{M}^{\alpha\beta}(\boldsymbol{q}) \right| i \right\rangle = \langle f | \gamma_{\alpha,\beta}(\boldsymbol{q}) | i \rangle + \sum_l \left(\frac{\langle f | j_\beta(\boldsymbol{k}_f) | l \rangle \langle l | j_\alpha(-\boldsymbol{k}_i) | i \rangle}{\varepsilon_l - \varepsilon_i - \omega_i} + \frac{\langle f | j_\alpha(-\boldsymbol{k}_i) | l \rangle \langle l | j_\beta(\boldsymbol{k}_f) | i \rangle}{\varepsilon_l - \varepsilon_i + \omega_f} \right) \tag{11}$$

with the sum l over intermediate states. After substituting into the cross-section formula, one obtains three terms in the cross-section: a nonresonant term; a mixed term; and a pure resonant term (because it is constructed from the square of the scattering operator). The components of the cross-section can be extracted from the appropriate correlation functions (response functions) first calculated on the imaginary Matsubara frequencies and then analytically continued onto the real axis [16]. Hence, we concentrate on the light-scattering response function $\chi(\boldsymbol{q},\Omega)$, which is related to the cross-section and has nonresonant, mixed and resonant contributions:

$$\begin{aligned} R(\boldsymbol{q},\Omega) &= \frac{2\pi g^2(\boldsymbol{k}_i) g^2(\boldsymbol{k}_f)}{1-\exp(-\beta\Omega)} \chi(\boldsymbol{q},\Omega), \\ \chi(\boldsymbol{q},\Omega) &= \chi_N(\boldsymbol{q},\Omega) + \chi_M(\boldsymbol{q},\Omega) + \chi_R(\boldsymbol{q},\Omega). \end{aligned} \tag{12}$$

Inelastic light scattering examines charge excitations of different symmetries by employing polarizers on both the incident and scattered light. The A_{1g} symmetry has the full symmetry of the lattice and is primarily measured by taking the initial and final polarizations to be $\boldsymbol{e}^i = \boldsymbol{e}^f = (1,1,1,1,\ldots)$. The B_{1g} symmetry involves crossed polarizers: $\boldsymbol{e}^i = (1,1,1,1,\ldots)$ and $\boldsymbol{e}^f = (-1,1,-1,1,\ldots)$; while the B_{2g} symmetry is rotated by 45 degrees; it requires the polarization vectors to satisfy $\boldsymbol{e}^i = (1,0,1,0,\ldots)$ and $\boldsymbol{e}^f = (0,1,0,1,\ldots)$. For Raman scattering ($\boldsymbol{q} = 0$), it is easy to show that for a system with only nearest-neighbor hopping and in the limit of large spatial dimensions, the A_{1g} sector has contributions from nonresonant, mixed and resonant scattering, the B_{1g} sector has contributions from nonresonant and resonant scattering only, and the B_{2g} sector is purely resonant [19, 20].

An analysis of the total electronic Raman spectra for the uniform phase of the Falicov–Kimball model has already been completed [16]. A full calculation of the nonresonant inelastic light scattering for all $\boldsymbol{q}$ in the CDW chess-board phase has also been presented [6]. Here we focus on the total response including the mixed and resonant contributions for the Raman scattering ($\boldsymbol{q} = 0$) in CDW phase.

IV. MIXED AND RESONANT RESPONSES

The way we determine the mixed and resonant response functions is as follows: we construct the corresponding multi-time correlation function in terms of the generalized polarizations, then perform a Fourier transformation to the imaginary Matsubara frequencies and finally analytically continue onto the real frequency axis to extract the response function. Such a procedure requires a lot of algebra and analysis [16]; we do not present all of the details here, but instead we summarize the main points.

The mixed response function is extracted from the multi-time correlation function which is built on three operators: one stress tensor and two current operators, as follows

$$\chi_{\tilde{\gamma},\tilde{f},\tilde{i}}(\tau_1,\tau_2,\tau_3) = \left\langle T_\tau \tilde{\gamma}(\tau_1) \tilde{j}^{(f)}(\tau_2) \tilde{j}^{(i)}(\tau_3) \right\rangle . \tag{13}$$

The symbol T_τ is a time ordering operator and the tilde denotes contractions with the polarization vectors [$\tilde{\gamma} = \sum_{\alpha\beta} e_\alpha^i \gamma_{\alpha,\beta}(\boldsymbol{q}) e_\beta^f$ and $\tilde{j}^{(i,f)} = \sum_\alpha e_\alpha^{i,f} j_\alpha(\mp\boldsymbol{k}_{i,f})$]. Furthermore, we perform the Fourier transformation from the imaginary times τ_1, τ_2, and τ_3 to the imaginary Matsubara frequencies $i\nu_i, i\nu_f$, and $i\nu_i - i\nu_f$. As a result, the correlation function is represented as a sum over Matsubara frequencies of the generalized polarizations $\Pi_{m+i,m+i-f,m}$:

$$\chi_{\tilde{\gamma},f,i}(i\nu_i - i\nu_f, i\nu_f, -i\nu_i) = T\sum_m \left[\Pi_{m-f,m+i-f,m} + \Pi_{m+i,m+i-f,m}\right], \quad (14)$$

where we introduced the shorthand notation $\Pi_{m-f,m+i-f,m} = \Pi(i\omega_m - i\nu_f, i\omega_m + i\nu_i - i\nu_f, i\omega_m)$ for the dependence on the fermionic $i\omega_m = i\pi T(2m+1)$ and bosonic $i\nu_l = i2\pi Tl$ Matsubara frequencies. In the case of a CDW ordered phase, the Feynman diagrams for the generalized polarizations $\Pi_{m,m+l}$ are shown in Fig. 1, where we introduce additional sublattice indexes a to s.

Now one has to carefully perform the analytic continuation to the real axis ($i\nu_{i,f} \to \omega_{i,f} \pm i0^+, i\nu_i - i\nu_f \to \Omega \pm i0^+$) and replace the sum over Matsubara frequencies by an integral over the real axis. Then the mixed response function is expressed directly in terms of the generalized polarizations

$$\begin{aligned}\chi_M(\boldsymbol{q},\Omega) = \frac{1}{(2\pi i)^2}\int_{-\infty}^{+\infty} d\omega\,[f(\omega) - f(\omega+\Omega)] \\ \times \mathrm{Re}\Big\{\Pi(\omega-\omega_f+i0^+,\omega+\Omega+i0^+,\omega-i0^+) - \Pi(\omega-\omega_f+i0^+,\omega+\Omega-i0^+,\omega-i0^+) \\ + \Pi(\omega-\omega_f-i0^+,\omega+\Omega+i0^+,\omega-i0^+) - \Pi(\omega-\omega_f-i0^+,\omega+\Omega-i0^+,\omega-i0^+) \\ + \Pi(\omega+\omega_i+i0^+,\omega+\Omega+i0^+,\omega-i0^+) - \Pi(\omega+\omega_f+i0^+,\omega+\Omega-i0^+,\omega-i0^+) \\ + \Pi(\omega+\omega_f-i0^+,\omega+\Omega+i0^+,\omega-i0^+) - \Pi(\omega+\omega_f-i0^+,\omega+\Omega-i0^+,\omega-i0^+)\Big\},\end{aligned} \quad (15)$$

where $f(\omega) = 1/[\exp(\beta\omega)+1]$ is the Fermi-Dirac distribution function.

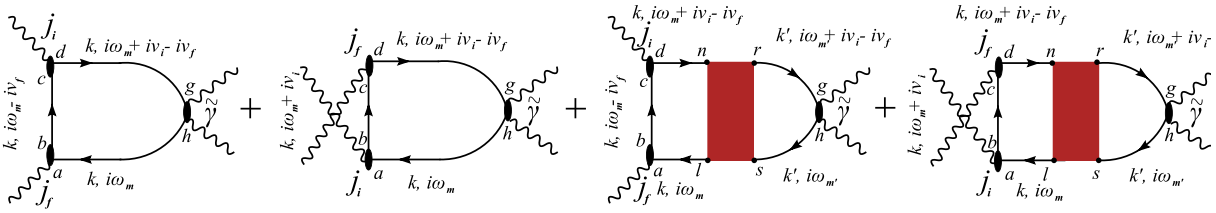

Fig. 1. Feynman diagrams for the generalized polarizations of the mixed response function. Due to the properties of the dynamic irreducible charge vertex of the Falicov–Kimball model, we have $m = m'$.

The mixed contribution is nonzero only for the A_{1g} symmetry; for other symmetries it vanishes after the summation over wave vectors. The next step is to calculate these generalized polarizations. There are two types of diagrams for the generalized polarizations (see Fig. 1): the bare loop and the renormalized loop. The reducible charge vertex $\tilde{\Gamma}^{ab}$ (shaded rectangle in Fig. 1) is defined from the Bethe-Salpeter-like equation through the irreducible one Γ_a which is local in the DMFT approach on each sublattice [6] and has the same functional form as in the uniform phase [21–23]. Also, we used the fact that the total reducible charge vertex is a diagonal function of frequencies for the Falicov–Kimball model [21–23]; for other models, where the vertex is no longer diagonal, the analysis is more complicated. The final expression for the generalized polarization is too cumbersome to be presented here.

Similar to the mixed response, the resonant response function is constructed from a multi-time correlation function which is built on four current operators

$$\chi_{i,f,f,i}(\tau_1,\tau_2,\tau_3,\tau_4) = \left\langle T_\tau j^{(i)}(\tau_1) j^{(f)}(\tau_2) j^{(f)}(\tau_3) j^{(i)}(\tau_4)\right\rangle. \quad (16)$$

Furthermore, we perform the same formal analytic continuation procedure as for the mixed response function. In Fig. 2, we present the Feynman diagrams for the generalized polarizations which contribute to the resonant response function.

For the resonant response function, the analytical continuation onto the real axis is quite complex, but the general method remains the same and the final formula for the resonant response function is similar to the mixed response function in Eq. (15) (see Ref. [16] for results in the normal phase). In contrast to the nonresonant and mixed response, the resonant response contributes to all symmetries. In addition, both the bare and renormalized loops in Fig. 2 are present in the resonant response function. In the B_{2g} symmetry we have only the resonant response, in the B_{1g} symmetry we have both nonresonant and resonant responses, and in the A_{1g} symmetry we have all three responses.

V. RESULTS AND CONCLUSIONS

A detailed analysis of the single particle DOS in the chessboard CDW phase of the Falicov–Kimball model

has been presented earlier [5]. Here we show results for Raman scattering in the CDW phase with $U = 2$ and temperature $T = 0.05$ (which lies below the critical temperature $T_c \approx 0.0769$). In Fig. 3, we show the DOS (left panel) and varying contributions to the Raman response for the A_{1g} and B_{1g} symmetries.

In Fig. 3 (a) one can see the main features of the DOS for chessboard phase at intermediate T: the gap of width U edged by singularities at $\omega = \pm U/2$ and partially filled by subgap states placed at $\omega = \pm E/2$ ($E \approx 1$ for the case of $U = 2$ and $T = 0.05$). As a result, the scattering spectra displays features (peaks) at frequencies $\Omega = (U - E)/2$, E, $(U + E)/2$, and U. Such features (peaks) were already observed for the optical conductivity [5] and for the nonresonant Raman and X-ray responses [6]. In addition, there can also be features at $\omega_i - U$, $\omega_i - (U + E)/2$, $\omega_i - E$, and $\omega_i - (U - E)/2$.

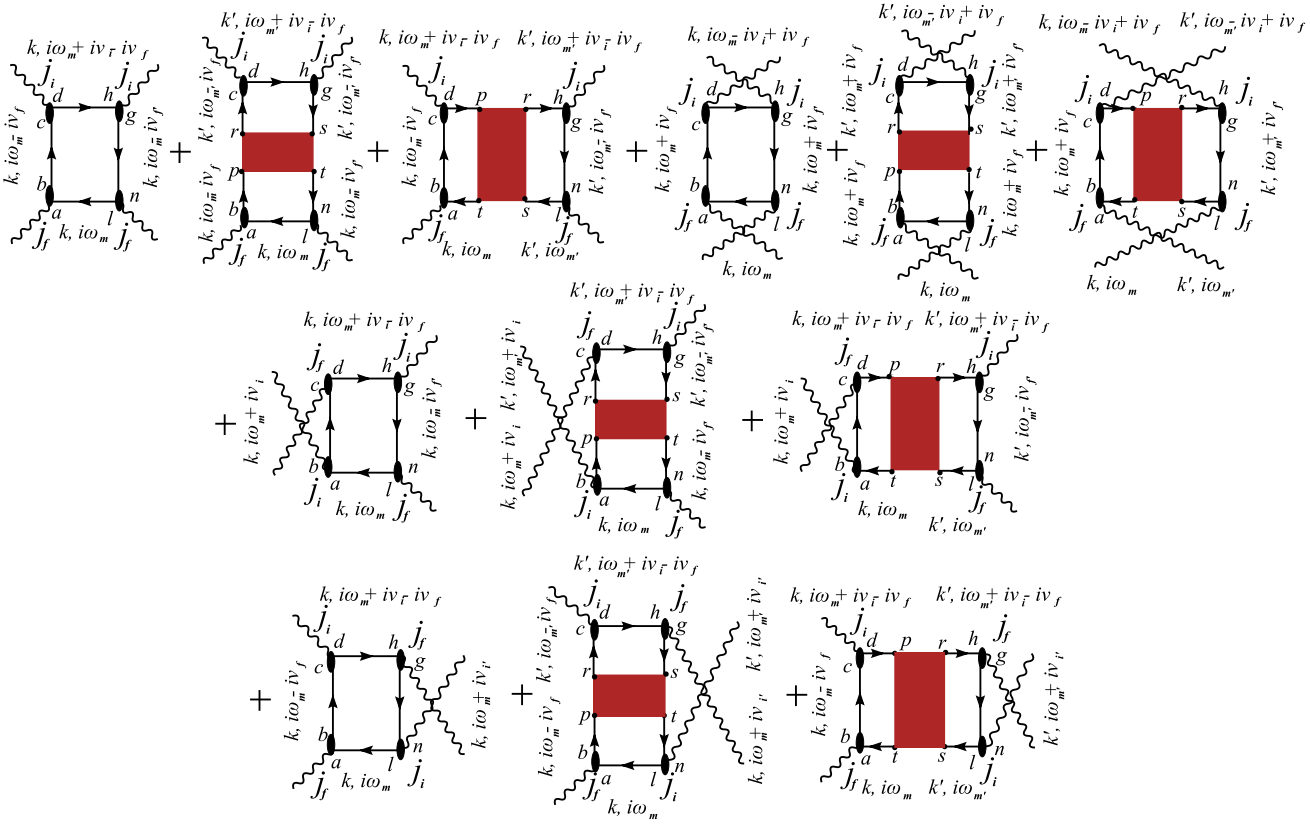

Fig. 2. Feynman diagrams for the generalized polarizations of the resonant response function. Both the renormalized and bare loop diagrams contribute in all symmetries (A_{1g}, B_{1g} and B_{2g}).

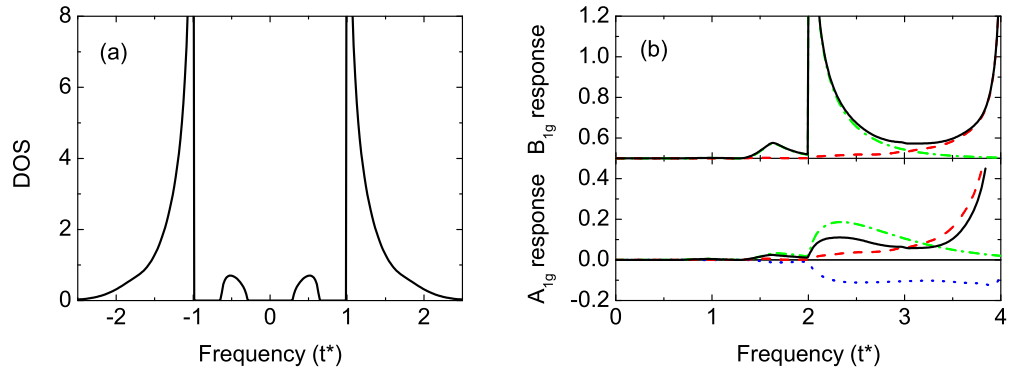

Fig. 3. (a) DOS and (b) different contributions to the Raman responses ($\omega_i = 4$) at $T = 0.05$ and $U = 2$. The solid line corresponds to the total response, the dashed-dotted line corresponds to the nonresonant contribution, the dashed line corresponds to the resonant contribution, and the dotted line corresponds to the mixed contribution.

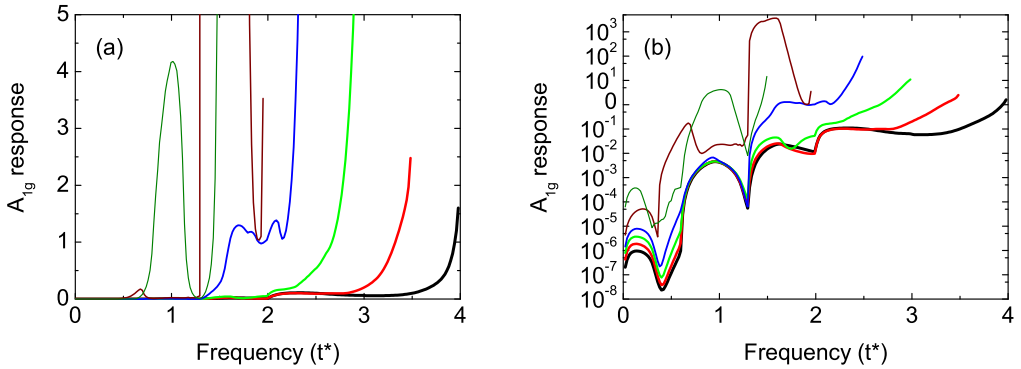

Fig. 4. Total Raman response for the A_{1g} symmetry at $T = 0.05$ for $U = 2$ on (a) a linear and (b) a logarithmic scale. Different curves correspond to different incident photon energies ranging from $\omega_i = 1.5$ to $\omega_i = 4.0$ in steps of 0.5.

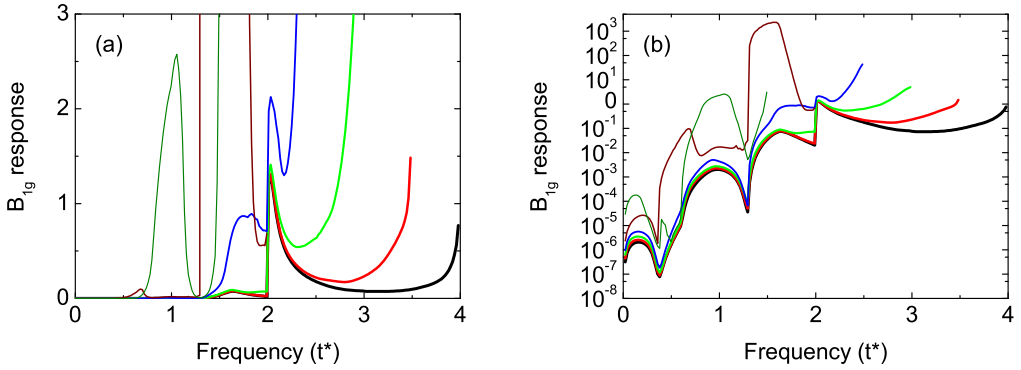

Fig. 5. Total Raman response for the B_{1g} symmetry at $T = 0.05$ for $U = 2$ on (a) a linear and (b) a logarithmic scale. Different curves correspond to different incident photon energies ranging from $\omega_i = 1.5$ to $\omega_i = 4.0$ in steps of 0.5.

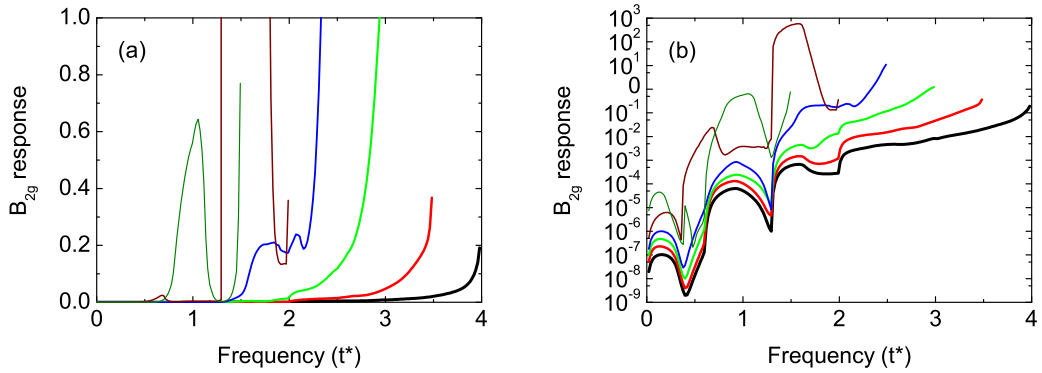

Fig. 6. Total Raman response for the B_{2g} symmetry at $T = 0.05$ for $U = 2$ on (a) a linear and (b) a logarithmic scale. Different curves correspond to different incident photon energies ranging from $\omega_i = 1.5$ to $\omega_i = 4.0$ in steps of 0.5.

In the case of B_{1g} symmetry [Fig. 3 (b)], there is a large peak in the nonresonant response at a frequency equal to $\Omega = U$ that reflects the transitions between the states above and below the gap. The peak has a square root-like singularity, that comes from the shape of DOS when there is CDW order and the fact that there is no screening for the nonresonant response in this symmetry channel. The smaller peak corresponds to transitions between states of the upper (bottom) band and the lower (upper) subgap states at $[\Omega = (U + E)/2]$. In addition to the nonresonant response, the resonant one has contributions from the renormalized charge excitations (Fig. 2) which reduce the high-energy transitions. As was mentioned above, all contributions contribute in the total response for the A_{1g} symmetry [Fig. 3 (b)]. Because of the charge renormalization in the nonresonant, mixed and resonant response functions, the total response is smaller than in the B_{1g} symmetry and there is no square root singularity.

The total Raman response is presented in set of Figs. 4–6 for the different symmetry channels and for different energies of the incident photons. One can see the

main features which were already observed for the optical conductivity and nonresonant scattering: four peaks at $\Omega = (U-E)/2$, E, $(U+E)/2$, and U which correspond to the different interband transitions. In addition, the resonant and mixed contributions strongly modify the nonresonant response: there is a strong enhancement of the scattering when the energy of the incident photon is close to the energy of the interband transitions and there is the appearance of additional features (peaks) at the frequencies $\Omega = \omega_i - U$, $\omega_i - (U-E)/2$, $\omega_i - E$, and $\omega_i - (U+E)/2$ as measured from the energy of the incident photon.

The resonant response is particularly large near the transferred energy $\Omega \approx 1.5$ when $\omega_i \approx 2$. By examining results on a finer grid of photon frequencies (not shown here) we establish that the resonant profile has a narrow full width at half max of much less than 0.1, and a very sharp dependence on ω_i (the peak height drops by more than three orders of magnitude by the time $\omega_i = 2.1$ or 1.9). In addition, the resonant response in this region does not depend too strongly on the symmetry channel of the scattering. Note how similar the curves appear (on a log scale) for the different symmetry channels, especially for transferred energies away from U where the gap edge creates sharp features in the B_{1g} channel. Finally, there are joint resonances, as the lower energy peaks do resonate with the large peak, especially for $\omega_i \approx 2$. Similar resonant effects can be seen for the lower-energy peaks when the incident photon frequency is lower, but they are not as dramatic as what happens for the peak near $\Omega \approx 1.5$. These resonant effects could be strong signatures of the CDW phase in real materials. The resonant enhancements in the normal phase do not produce such enormous peaks or have such sharp dependences on the incident photon frequencies; this behavior is arising predominantly from the CDW order.

In conclusion, we have examined the total electronic Raman scattering response for the spinless Falicov–Kimball model in the ordered CDW phase. Space limitations allowed us to only consider one value of the interaction and temperature, but we see some interesting results, primarily the appearance of a huge resonantly enhanced peak near $\omega_i = U$ that is essentially independent of the symmetry channel. Such a peak could be an important signal for experiments on these systems as indicating the appearance of the CDW phase via a direct measurment of the electronic charge dynamics. Future work will elaborate on how these features evolve with U and T and will provide additional details of the formalism that could not be included here.

VI. ACKNOWLEDGMENTS

J. K. F. was supported by the Department of Energy, Office of Basic Energy Sciences, under grant number DE-FG02-08ER46542. The collaboration was supported by the Computational Materials Science Network (CMSN) program of the Division of Materials Science and Engineering, Basic Energy Sciences, U. S. Department of Energy under grant number DE-FG02-08ER46540.

[1] S. Tajima, S. Uchida, A. Masaki, H. Takagi, K. Kitazawa, S. Tanaka, A. Katsui, Phys. Rev. B **32**, 6302 (1985).
[2] M. A. Karlow, S. L. Cooper, A. L. Kotz, M. V. Klein, P. D. Han, D. A. Payne, Phys. Rev. B **48**, 6499 (1993).
[3] S. M. Hasanuzzaman, Kaoru Iwano, Keiichiro Nasu, J. Phys. Soc. Jpn **68**, 1376 (1999).
[4] S. R. Hassan, H. R. Krishnamurthy, Phys. Rev. B **76**, 205109 (2007).
[5] O. P. Matveev, A. M. Shvaika, J. K. Freericks, Phys. Rev. B **77**, 035102 (2008).
[6] O. P. Matveev, A. M. Shvaika, J. K. Freericks, Phys. Rev. B **79**, 115130 (2009).
[7] L. M. Falicov, J. C. Kimball, Phys. Rev. Lett. **22**, 997 (1969).
[8] U. Brandt, C. Mielsch, Z. Phys. B: Condens. Matter **75**, 365 (1989).
[9] J. K. Freericks, V. Zlatić, Rev. Mod. Phys. **75**, 1333 (2003).
[10] U. Brandt, C. Mielsch, Z. Phys. B: Condens. Matter **79**, 295 (1990).
[11] W. Metzner, D. Vollhardt, Phys. Rev. Lett. **62**, 324 (1989).
[12] P. G. J. van Dongen, Phys. Rev. B **45**, 2267 (1992).
[13] L. Chen, J. K. Freericks, B. A. Jones, Phys. Rev. B **68**, 153102 (2003).
[14] C. Gruber, N. Macris, P. Royer, J. K. Freericks, Phys. Rev. B **63**, 165111 (2001).
[15] A. M. Shvaika, O. Vorobyov, J. K. Freericks, T. P. Devereaux, Phys. Rev. Lett. **93**, 137402 (2004).
[16] A. M. Shvaika, O. Vorobyov, J. K. Freericks, T. P. Devereaux, Phys. Rev. B **71**, 045120 (2005).
[17] B. S. Shastry, B. I. Shraiman, Phys. Rev. Lett. **65**, 1068 (1990).
[18] B. S. Shastry, B. I. Shraiman, Int. J. Mod. Phys. B **5**, 365 (1991).
[19] J. K. Freericks, T. P. Devereaux, Condens. Matter Phys. **4**, 149 (2001).
[20] J. K. Freericks, T. P. Devereaux, Phys. Rev. B **64**, 125110 (2001).
[21] A. M. Shvaika, Physica C **341–348**, 177 (2000).
[22] J. K. Freericks, P. Miller, Phys. Rev. B **62**, 10022 (2000).
[23] A. M. Shvaika, J. Phys. Stud. **5**, 349 (2001).

ПОВНЕ ЕЛЕКТРОННЕ КОМБІНАЦІЙНЕ РОЗСІЯННЯ СВІТЛА В ЗАРЯДОВОВПОРЯДКОВАНІЙ ФАЗІ БЕЗСПІНОВОЇ МОДЕЛІ ФАЛІКОВА–КІМБАЛА

О. П. Матвєєв[1], А. М. Швайка[1], Дж. К. Фрірікс[2]
[1] *Інститут фізики конденсованих систем НАН України, вул. Свєнціцького, 1, 79011, Львів, Україна*
[2] *Фізичний факультет, університет Джорджтауну, Вашингтон, DC 20057, США*

Для безспінової моделі Фалікова–Кімбала на гіперкубічній ґратці з подвійною модуляцією густини заряду при половинному заповненні в межах теорії динамічного середнього поля розраховано повні спектри комбінаційного розсіяння світла з урахуванням нерезонансних, змішаних та резонансних внесків. Досліджено їхні частотні залежності для різних енергій фотонів падаючого світла. Отримані спектри відображають наявність різних структур на густині станів та їхню зміну внаслідок динамічного екранування та резонансних ефектів. Усі розрахунки виконані для типових для експерименту симетрій A_{1g}, B_{1g} та B_{2g}. Одержані результати з резонансних ефектів у спектрах комбінаційного розсіяння, які отримано при зміні енергії налітаючих фотонів, дають інформацію про багаточастинкову зарядову динаміку в зарядововпорядкованій фазі.